Materials Advances

ROYAL SOCIETY OF CHEMISTRY

PAPER

View Article Online
View Journal | View Issue

Cite this: *Mater. Adv.*, 2023, 4, 5273

Green synthesis of *Mesona Blumes* gum capped silver nanoparticles and their antioxidant, antibacterial and catalytic studies†

Walaa Abdullah Sulaiman Al Yahyai,[a] Aya Ali Sulaiman Al Isai,[a] Mohammed F Alotibi,[b] Bhagavanth Reddy G,[c] Mohammed Al-Abri,[de] Babu Pejjai,[f] Nagaraju Devunuri,[g] Nadavala Siva Kumar,[h] Ahmed S. Al-Fatesh,[h] Ahmed I. Osman*[i] and Kondaiah Seku*[a]

Economically viable and eco-friendly *Mesona Blumes* (M.B.) gum was employed to synthesize AgNPs. The synthesis parameters such as concentration of silver nitrate ($AgNO_3$), M.B. gum, microwave irradiation time and pH effect were optimized using a UV-visible spectrophotometer. It was observed that increasing the concentration of silver nitrate ($AgNO_3$), M.B. gum, and microwave irradiation time enhanced the formation of MB@AgNPs. Fourier transform infrared spectroscopy (FTIR), X-ray powder diffraction (XRD), and transmission electron microscopy (TEM) techniques were used to characterize the synthesized MB@AgNPs. The XRD results confirmed a face-centred cubic structure, whereas TEM analysis indicated spherical particles of size 10 nm ± 2 nm. The majority of AgNPs were smooth and spherical, and very few were irregular. The catalytic efficacy of the MB@AgNPs was studied in the presence of $NaBH_4$ for the reduction of crystal violet (CV) and rhodamine-B (Rh-B) dyes. Rh-B dye was reduced in 300 seconds, while CV dye was reduced in 280 seconds. The inhibition zones of *Staphylococcus aureus*, *Bacillus subtilis*, *Escherichia coli*, and *Bacillus cereus* for the MB@AgNPs were 14, 12, 15, and 11 mm, respectively. The DPPH radical scavenging ability of the AgNPs was assessed using a DPPH radical scavenging assay.

Received 27th February 2023,
Accepted 16th September 2023

DOI: 10.1039/d3ma00091e

rsc.li/materials-advances

1. Introduction

The textiles, paint, paper, pulp and food industries are the major consumers of colourants and dyestuffs.[1] The dye effluents released in water usually contain toxic organic chemicals.[2] The dyes commonly found in effluents from process industries include rhodamine-B–B, methyl orange, methyl blue, crystal violet, methylene red, *etc.* Light cannot penetrate the surface when dyes accumulate in the water, affecting plant photosynthesis.[3] This causes the depletion of oxygen content in the water, resulting in aquatic life and plants dying.

The majority of dyes and pollutants are complex, non-biodegradable, and very difficult to decompose. Water contamination can be treated through different methods such as ultrafiltration, electrochemical, coagulation, physisorption, chemical precipitation, and ion exchange processes.[4–6] A variety of natural and synthetic adsorbents can also be used to remove pollutants from wastewater, such as coconut fibres and jute, *etc.*[7] However, the conventional methods are not feasible due to their slow process, incomplete removal of pollutants, and high operating costs *etc.* Therefore, the robust and efficient removal of industrial effluents and organic pollutants from water bodies is essential to maintain a healthy environment.

$NaBH_4$, along with nanoparticles or nanocomposites, is reported as an efficient and rapid method of eliminating organic pollutants from wastewater.[8,9] Several metal nanoparticles such as Ag, Au, ruthenium, nickel, Cu[10,11] and metal

[a] *Department of Engineering, Civil Section, University of Technology and Applied Sciences, Shinas, Sultanate of Oman. E-mail: kondaiah.seku@utas.edu.om*
[b] *Institute of Refining and Petrochemicals Technologies, King Abdulaziz City for Science and Technology (KACST), P. O. Box 6086, Riyadh 11442, Kingdom of Saudi Arabia*
[c] *Department of Chemistry, Palamuru University P.G. Centre, Wanaparthy, Telangana, Hyderabad, India*
[d] *Nanotechnology Research Center, Sultan Qaboos University, Muscat, Oman*
[e] *Department of Petroleum and Chemical Engineering, College of Engineering, Sultan Qaboos University, Muscat, Oman*
[f] *Department of Physics, Sri Venkateshwara College of Engineering, Karakambadi Road, Tirupati, 517507, India*
[g] *Department of Chemistry, School of Applied Sciences & Humanities, Vignan's Foundation for Science, Technology & Research (VFSTR) Deemed University, Guntur, India*
[h] *Department of Chemical Engineering, College of Engineering, King Saud University, P. O. Box 800, Riyadh 11421, Saudi Arabia*
[i] *School of Chemistry and Chemical Engineering, Queen's University Belfast, Belfast BT9 5AG, Northern Ireland, UK. E-mail: aosmanahmed01@qub.ac.uk*

† Electronic supplementary information (ESI) available. See DOI: https://doi.org/10.1039/d3ma00091e

oxide nanoparticles (ZnO, TiO_2, *etc.*) have been used for the degradation of organic pollutants.[12] It has been reported[13] that GO/MOF composites can eliminate organic contaminants from wastewater by Fuhua WeiIDet *et al.*, 2021. Recent literature shows that the use of AgNPs has remarkable potential in the degradation of organic pollutants due to their remarkable properties, including high chemical activity and unique interfacial interactions.[14] In addition, the smaller size enhances the surface area, enhancing the catalytic activity. A capping agent is present on the conjugate, allowing AgNPs to disperse uniformly on the sponge surface without clumping together. Catalysts made from nanoparticles are easily separated.

Therefore, researchers have focused on the synthesis of silver nanoparticles as silver nanoparticles are extensively used in industrial, biomedical, and pharmaceutical fields.[15] The synthesis of silver nanoparticles using natural and synthetic stabilization systems has been reported by various preparation methods such as chemical, physical, biological, *etc.*[16–19] The chemical process of synthesizing silver nanoparticles is expensive and environmentally hazardous, whereas the physical method is complex, time-consuming, and requires expensive equipment. However, the biogenic synthesis of metal nanoparticles has several advantages: simplicity, less-economic, environmental friendliness, and reliability. This synthetic route also encompasses the use of several biogenic macromolecules that act as capping agents and stabilizers.[20] Silver nanoparticle synthesis has also been reported using natural gums, leaf extract, and microorganisms.[21] It is novel that *Mesona Blumes* (M.B.) gum extract was used in this study to study the synthesis of silver nanoparticles without the use of expensive or toxic techniques. The gum comprises 9.74% protein, 30.89% ash, 2.98% crude fibre, and 42.19% sugar (w/w). It contains mostly arabinose, glucose, galactose, and uronic acid as monosaccharides.[22] Functional groups of the gum effectively act as capping and reducing agents for the synthesized AgNPs.[23] Since biogenic silver metal nanoparticles are highly efficient, low-cost, and simple to produce, they were considered to be highly promising for wastewater remediation. Silver nanoparticles derived from plant extracts have a greater advantage regarding their catalytic properties. The microwave irradiation method is a simple and ultra-fast technique for synthesizing metal nanoparticles. Therefore, microwave irradiation (M.W.) was used to prepare AgNPs using M.B. gum. A UV-Vis spectrophotometer was used to carry out MB@AgNP optimization experiments, while FTIR, XRD, and TEM were employed to characterize the synthesized MB@AgNPs.

In addition to water contamination by dyes, people are becoming resistant to multiple drugs due to unintentional overuse of antibiotics.[24] Multidrug resistance now affects the entire world and is challenging to overcome. The multidrug resistance of bacteria makes antibiotics ineffective in preventing diseases. Silver nanoparticles' antimicrobial and anticancer properties can be useful in overcoming multidrug resistance issues.[24] Therefore, in the present study, the antioxidant and antibacterial properties of the synthesized MB@AgNPs have also been tested in addition to dye degradation. It was found that bacterial cells were effectively disfunctionalized with MB@AgNPs. The synthesized MB@AgNPs were employed as a catalyst for the reduction of Rh-B and CV dyes in the presence of $NaBH_4$. The antibacterial activity of the MB@AgNPs was evaluated against *Staphylococcus aureus*, *Bacillus subtilis*, *Escherichia coli*, and *Bacillus cereus.* In addition, the antioxidant activity of the MB@AgNPs was studied.

2. Experimental details

2.1. Materials

The gum was purchased from Telangana Girijana Cooperative Society, Telangana State, India. Analytical grade chemicals and reagents ($AgNO_3$, $NaBH_4$, Crystal violet and rhodamine-B dye) were used in this study, acquired from Sigma Aldrich and SD Fine-Chem Limited (Mumbai, India).

2.2. Preparation of M.B. gum extract

1 gram of M.B. gum powder was added to 100 mL of distilled water and sonicated at room temperature for 10 minutes. Whatman filter paper was used to filtrate the gum solution and utilized to synthesize AgNPs.

2.3. Biosynthesis of AgNPs with Salmalia Malabarica gum extract

15 mL of M.B. gum extract was mixed with 15 mL of 1.5 mM $AgNO_3$ solution in a beaker. 450 Watts of microwave irradiation were applied to the reaction mixture for 160 seconds. After microwave irradiation, the mixture turned yellowish-orange colour,[25] which implies the development of silver nanoparticles.

2.4. Purification of AgNPs from the mixture

The yellowish-orange suspension mixture was centrifuged at 10 000 rpm for 30 minutes. The supinated filtrate was decanted, and the residue was redispersed in Milli-Q water. A centrifugation and scattering procedure were repeated twice in order to remove the unreacted $AgNO_3$ and Salmalia Malabarica gum extract solution from the product. The obtained purified AgNPs were dried at 60 °C in a hot air oven. The ESI† presents catalytic reduction, antioxidant, and antibacterial processes.

3. Results and discussion

3.1. UV-Visible absorption spectroscopic analysis

The synthesized MB@AgNPs were monitored with a UV-visible absorption spectrophotometer by evaluating the changes in solution colour.[26] Microwave irradiation of the Ag^+ ion solution results in a change in colour from colourless to yellowish orange. AgNPs are formed by the reduction of Ag^+ to Ag^0. The absorption peak of the MB@AgNPs was observed at 423 nm (Fig. 1a). Synthesized AgNPs were optimized using gum concentration, $AgNO_3$ concentration, microwave irradiation time and the effect of pH. A UV-visible spectroscopy study was conducted by varying the concentration of M.B. gum solution by maintaining a constant

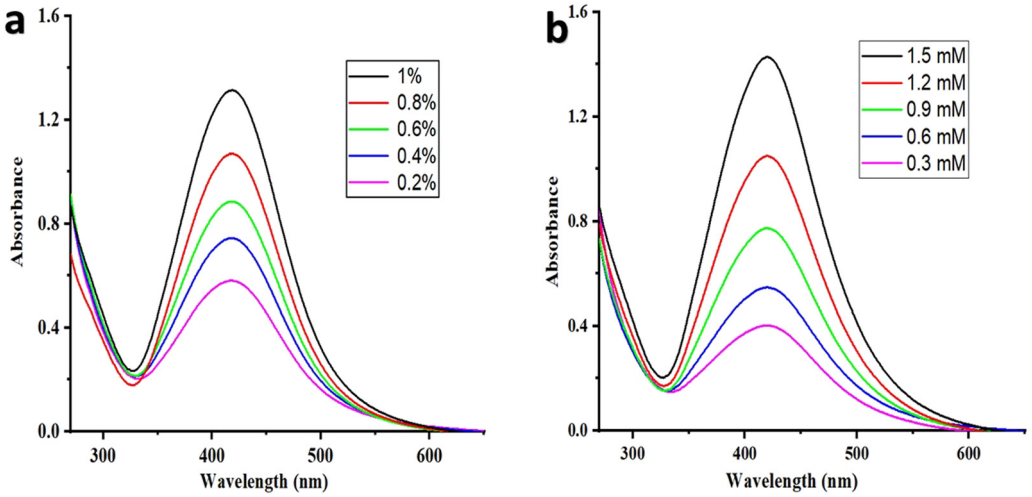

Fig. 1 UV-visible absorption spectra of MB@AgNPs (a) at different concentrations of the MB gum solution and (b) at various concentrations of $AgNO_3$ solution.

$AgNO_3$ concentration of 1.5 mM for 160 seconds of MWI.[27] The absorbance intensity of the AgNPs at 423nm (Fig. 1a) increased with M.B. gum concentration (0.2 to 1%), implying the formation of MB@AgNPs. An increase in the concentration of M.B. gum resulted in a large quantity of phytochemicals that reduced Ag^{+1} to Ag^0 and stabilized the AgNPs. In addition, the effect of $AgNO_3$ concentration on MB@AgNP synthesis was investigated by varying the $AgNO_3$ concentration (0.3–1.5 mM) by maintaining a constant concentration of M.B. solution (1%) for a MWI time of 160 s. The absorbance intensity increased (Fig. 1b) with the increase of the $AgNO_3$ concentration, which indicated the good yield of MB@AgNPs formation in the solution. The effect of MWI time (40, 80, 120, 160 seconds at 450 W) on MB@AgNPs was investigated at 1% M.B. gum solution and 1.5 mM of $AgNO_3$.[28] Fig. 2a shows that the absorbance intensity was increased with an increase in microwave irradiation. This indicates that the reducing ability (Ag^+ to Ag^0) of M.B. gum increased with microwave irradiation time.[29] From UV-visible spectroscopic optimization studies, it is concluded that the maximum yield of AgNPs was obtained for the conditions of 160 s irradiation time with 1% M.B. gum solution and 1.5 mM of $AgNO_3$.

The effect of pH on AgNPs production was also investigated. Fig. 2b shows the UV-Vis spectra of AgNPs prepared at various pH values of gum solution (3, 4, 5, 6, 8, 10, and 11). When the pH value increased, the peak intensity increased gradually. This indicates the ionization of more functional groups in the gum; consequently, the rate of silver ion reduction was also increased.[30] Even after a pH value of 11, the peak intensity remained constant. In the present study, a large amount of AgNPs was formed at pH = 11.

3.2. FTIR analysis

M.B. becomes a complex with Ag(I) through its hydroxyl and carbonyl functions. A strong antioxidant nature and a high

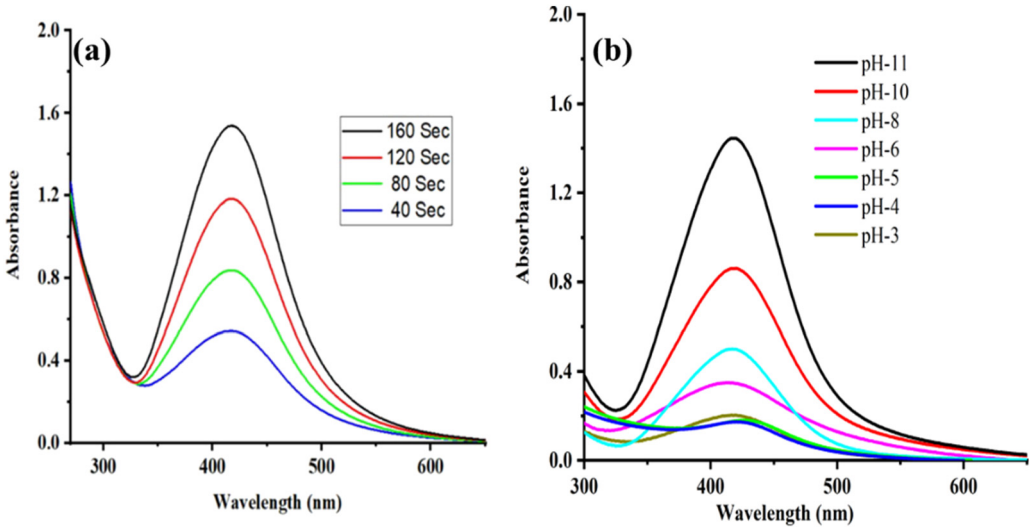

Fig. 2 (a) UV-visible absorption spectrum of MB@AgNPs varying with microwave exposure time and (b) AgNPs synthesized in different pH conditions.

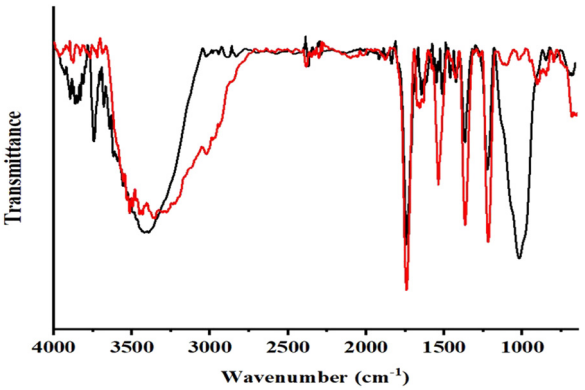

Fig. 3 FTIR spectra of (a) MB gum (red colour) and (b) MB@AgNPs (black colour).

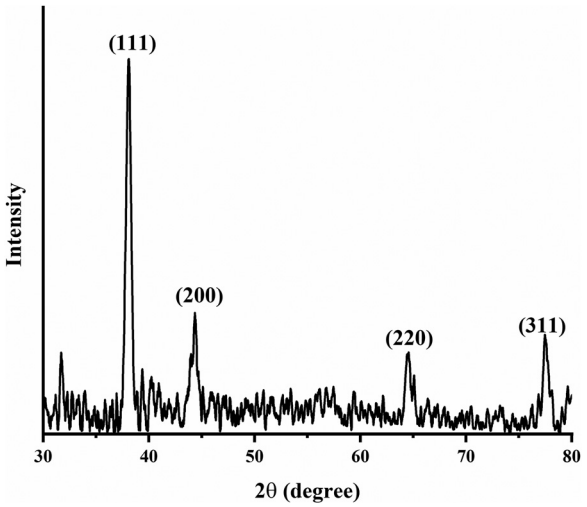

Fig. 4 Powder X-ray diffraction pattern of MB@AgNPs.

reducing capacity are responsible for reducing Ag^{+} atoms to Ag^{0} atoms through these hydroxyl and carbonyl functions. In order to grow AgNPs, Ag atoms serve as nucleation sites. In these phytochemicals, oxygen-containing functional groups are bound to metal atoms on the surfaces, thereby controlling and stabilizing the size of the AgNPs. Fig. 3 shows the FTIR analysis of M.B. gum before and after AgNP synthesis, confirming this hypothesis.[31] Formation and stabilization of MB@AgNPs by the hydroxyl and carbonyl groups of M.B. gum. The intensities of the hydroxyl and carbonyl groups and carboxyl peaks were found to be decreased.

The FTIR spectra were recorded in the 400–4000 cm^{-1} range on a Shimadzu IR Affinity-1 using the KBr pellet method. FTIR measurements were used to assess the active functional groups in M.B. gum solution and their role in reducing and stabilizing AgNP formation. FTIR spectra of M.B. gum and MB@AgNPs were compared. A broad peak was observed at 3445 cm^{-1} in the FTIR spectrum of M.B. (Fig. 3 – red colour line), as well as a sharp stretching peak at 1750 cm^{-1}, which indicates the presence of hydroxyl and carbonyl functional groups.[32] Additionally, it exhibited strong characteristic peaks at 1500, 1400, and 1200 cm^{-1}, which correspond to vibrations of C=C, O–H (bending), and C–O stretching. In the FTIR spectrum of MB@AgNPs (Fig. 3 – black line), the intensities of the peaks of hydroxyl and carbonyl groups and a new carboxyl peak at 1700 cm^{-1} were decreased. Similarly, the peak intensities of C–C (bending), O–H (bending) and C–O stretching vibrations were also decreased.[33] Silver nanoparticles can be formed by binding with the functional groups of M.B. gum, as indicated by changes in the peak intensities in the spectrum of the MB@AgNPs. The reduction and stabilization of AgNPs was attributed to M.B. gum functional groups.

3.3. Powder XRD studies

A powder XRD study was performed on the MB@AgNPs to determine their crystallinity and structure. XRD (Fig. 4) showed four characteristic peaks at 2θ values of 39.65°, 45.24°, 65.14°, and 78.65° and these peaks were indexed to the (111), (200), (222) and (311) planes of the face-centered cubic structure of Ag (JCPDS-File No. 04-0783), respectively. The XRD pattern showed the (111) peak as the most intense,[34] which indicates the predominant growth of AgNPs in the (111) orientation. The obtained highly intense peaks in the XRD pattern of the MB@AgNPs indicate the good crystalline nature of the synthesized MB@AgNPs.

The average crystallite size of the MB@AgNPs was calculated using Scherrer's equation[25]

$$D = k\lambda/\beta\cos\theta$$

where λ = wavelength, θ = Bragg angle, β = full width at half maximum of the strongest peak, and k = shape-dependent Scherrer's constant.[32] The calculated average crystallite size of the MB@AgNPs was found to be 8.49 nm.

3.4. TEM studies

To further confirm the size and shape of the MB@AgNPs, TEM analysis was carried out on MB@AgNPs. Fig. 5a shows TEM images of MB@AgNPs. TEM images showed spherical shape nanoparticles of the synthesized MB@AgNPs. The spherical AgNPs were not agglomerated, indicating the effective capping and stabilizing effect of the M.B. gum material. Fig. 5c shows a high-resolution TEM image of the synthesized AgNPs and clear lattice fringes, indicating that the synthesized nanoparticles were crystalline (Fig. 5b). SAED patterns of nanoparticles produced by the selected-area electron diffraction technique are shown in Fig. 5b, which confirms their highly crystalline nature. The rings are caused by diffraction from a face-centered cubic (FCC) silver plane (111), (200), (220) and (311). Fig. 5d shows the developed histogram using 150 nanoparticles. The particle size histogram of MB@AgNPs (Fig. 5b) showed an average diameter of 10 nm (± 2 nm), which is well matched with the crystallite size calculated from XRD. The TEM image showed well-dispersed MB@AgNPs with a smooth surface without any aggregation. The MB gum layer on the surface of the AgNPs prevented aggregation.[35]

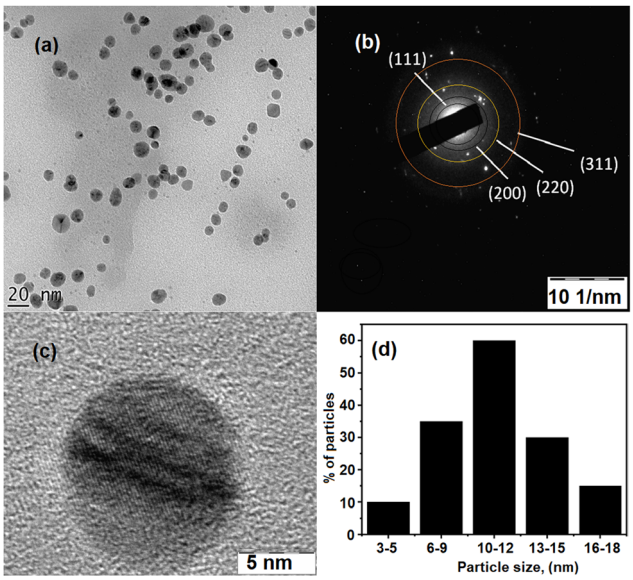

Fig. 5 (a) TEM image of MB@AgNPs and (b) SAED pattern of MB@AgNPs; (c) 5 nm of MB@AgNPs; and (d) particle size distribution histogram of MB@AgNPs.

3.5. Catalytic reduction of crystal violet dye

In this study, MB@AgNPs are used to reduce CV dye with $NaBH_4$ catalytically. The CV dye showed the following absorption peaks at 600, 305, and 250 nm in the UV-visible spectrophotometer.[36] As shown in Fig. 6a, a change in the peak intensity was not detected even after 45 minutes with the addition of $NaBH_4$ to the CV dye solution. This concluded that $NaBH_4$ alone was not effective in reducing CV dye completely. A complete reduction of CV dye was achieved by adding MB@AgNPs to the above reaction. After the addition of MB@AgNPs, the intensity of the absorbance peaks (563, 305, and 250 nm) was found to be rapidly decreased (Fig. 6b). Upon completion of CV dye reduction, the blue colour of the CV dye solution turned colourless,[37] which confirms the catalytic efficacy of the synthesized MB@AgNPs.[38] We found that MB@AgNPs have reduced CV dye effectively (95%). The reduction reaction progress was traced using a linear relationship between ln (A_t/A_0) and reaction time (Fig. 6c). It showed pseudo-first-order kinetics at room temperature, and the rate constant was 0.026 s^{-1}. The influence of catalyst quantity was investigated in the 6–10 mg range. The rate constants for 6, 7, 8, 9, and 10 mg MB@AgNPs are 0.024, 0.026, 0.029, 0.033, and

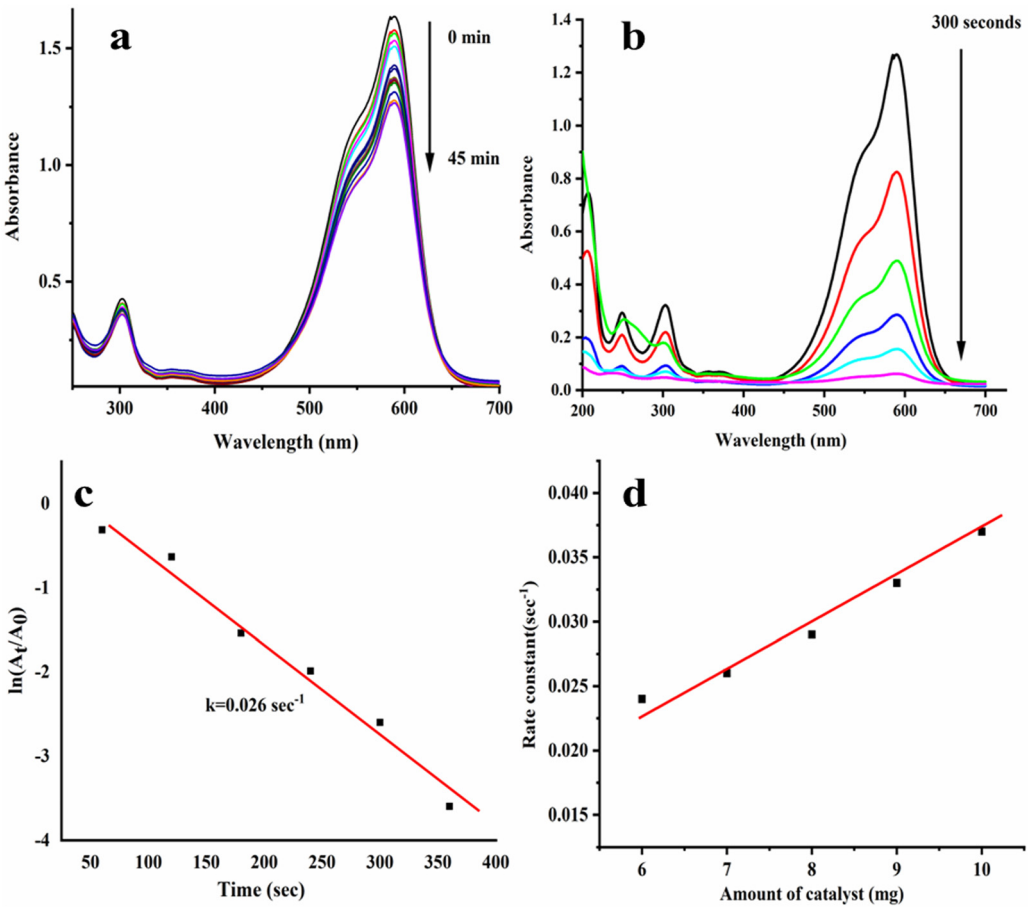

Fig. 6 UV-Visible spectra of CV dye reduction: (a) in the presence of $NaBH_4$ only, (b) in the presence of $NaBH_4$ and MB@AgNPs, (c) the plot of log (A_t/A_0) *versus* reaction time, and (d) plot of rate constant (k) *versus* amount of MB@AgNPs.

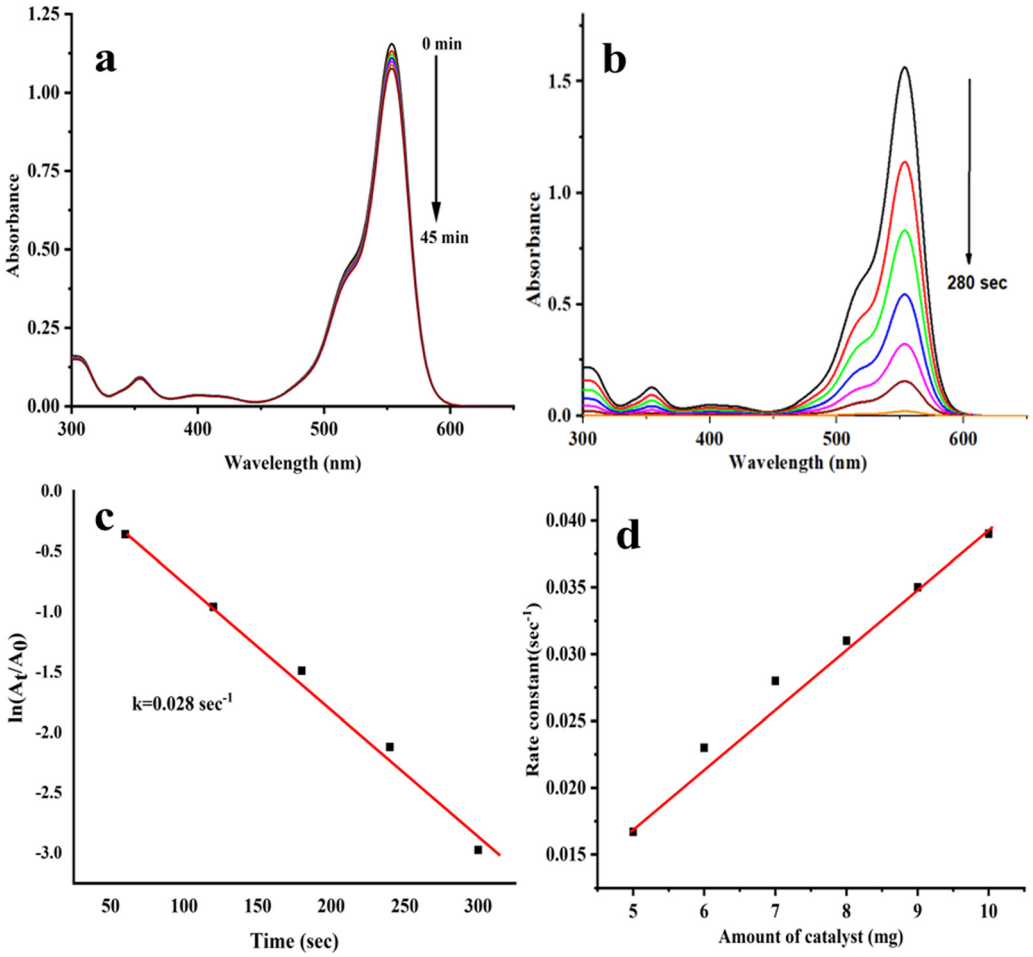

Fig. 7 (a) Absorption spectra of Rh-B in the presence of $NaBH_4$ in the absence of MB@AgNPs, (b) time-dependent UV-Vis spectra of Rh-B reduction with $NaBH_4$ and MB@AgNP catalysts, (c) linear plot of (A_t/A_0) *vs.* time for Rh-B reduction, and (d) plot of rate constant (*k*) *versus* amount of BM@AgNPs.

0.037 s^{-1}, respectively. As anticipated, the constant was increased with the increase of the MB@AgNPs quantity (Fig. 6d) in the reaction due to the increased number of reaction sites.

3.6. Catalytic reduction of Rh-B Dye

A wide range of applications for Rh-B is found in industry, such as printing and dyeing fabrics, paper, paint, leather, *etc.* Rh-B dye is soluble in water, and it is chemically basic. However, it can cause severe health problems, including irritated skin and eyes, as well as cancer. MB@AgNPs and $NaBH_4$ were used to investigate the catalytic degradation of Rh-B dye. An absorption peak at 550 nm was observed in the Rh-B reduction when catalyzed by $NaBH_4$. The peak at 550 nm remains constant even after 60 minutes in the case of Rh-B + $NaBH_4$ (Fig. 7a), which suggests that $NaBH_4$ alone could not be able to reduce Rh-B efficiently[39,40] However, the Rh-B reduction was achieved quickly (in 280 seconds) in the presence of MB@AgNPs. When the reaction time was increased, the intensity of the absorption bands at 550 nm was decreased (Fig. 7b). A change in dye colour to colourless was observed.[41,42] Rh-B was 95% reduced in the presence of MB@AgNPs.[43] The reaction time (Fig. 7c) was calculated using $\ln(A_t/A_0)$, which indicates pseudo-first-order kinetics with a rate constant of 0.028 s^{-1} at room temperature.[44] Our studies found that MB@AgNPs are more active due to their larger surface-to-volume ratio, high surface coverage, improved electron transfer properties, and efficacy in reducing the kinetic barriers of the reduction reactions.[45] The role of the amount of catalyst was investigated in the range of 6–10 mg. The rate constants for 5, 6, 7, 8, 9, and 10 mg of

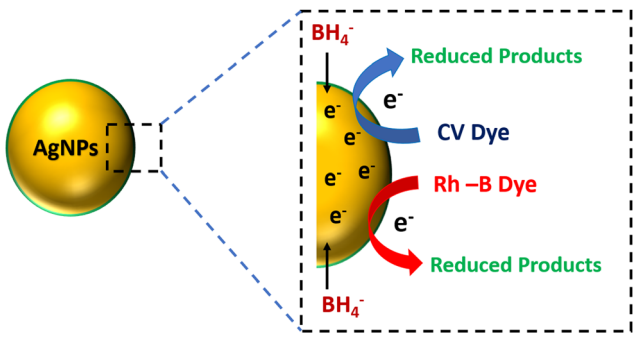

Fig. 8 CV and Rh-B dye catalytic reduction mechanism by MB@AgNPs in the presence of $NaBH_4$.

Table 1 Comparative study of MB@AgNPs and previously reported catalysts for CV and Rh-B reduction

Name of the dye	Catalyst	Time	Ref.
Rh-B	Bael gum@AgNPs	10 min	46
	MC-PDA-Ag	20 min	8
	ANL@AuNPs	120 min	47
	Colocasia esculentaAgNPs	7 min	48
	MB@AgNPs	**4 min 40 s**	**This work**
CV	Gumarabic@CuNPs	20 min	49
	PtNPs	15 min	50
	g-CN decorated with AgNPs	8 min	51
	MB@AgNPs	**5 min**	**This work**

MB@AgNPs are 0.0134, 0.023, 0.028, 0.031, 0.035, and 0.039 s^{-1}, respectively. As anticipated, the constant was increased with the increase of the MB@AgNPs amount (Fig. 7d) due to an increase in the number of reaction sites.

3.7. The catalytic reduction mechanism of the dyes

Fig. 8 illustrates CV and Rh-B dye's possible catalytic reduction mechanism using MB@AgNPs as the catalyst. The first stage of the reduction process results in $NaBH_4$ adsorbing on the surface of the MB@AgNPs. These molecules include CV and Rh-B dye molecules from the analyte. By electrostatic interactions, AgNPs transfer electrons from BH^{4-} (donor) to analytes (acceptor), and all of these reactions occur at the surface of the AgNPs. The electron transfer will reduce the analytes on the surface of the AgNPs.[23] The by-products formed diffused into the bulk of the solution after being desorbed from the AgNP surface. In Table 1, we compared the catalytic activity of the MB@AgNPs with catalysts reported in the previous literature.

3.8. Recyclability of the MB@AgNP catalyst

The reusability of the MB@AgNP catalysts in various reduction processes of CV and Rh-B dyes was investigated. A vacuum oven was used to dry and clean the catalyst after being cleaned and dried in water and ethanol. MB@AgNPs can be recycled for reduction reactions of CV and Rh-B dyes, respectively, as shown in Fig. 9a and b. MB@AgNPs showed very little loss of catalytic activity after five cycles in the reduction of CV and Rh-B dyes, which indicates that the catalyst is highly stable.

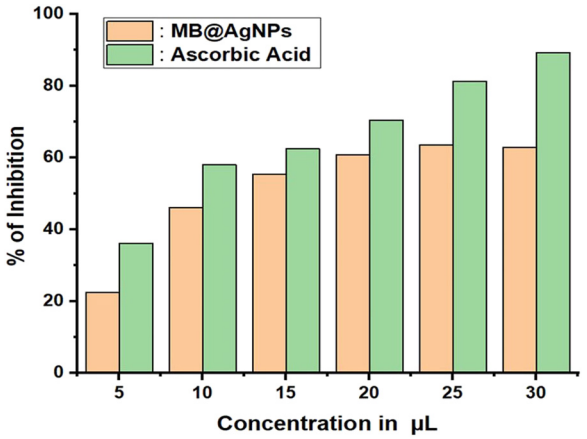

Fig. 10 Antioxidant activity of MB@AgNPs.

3.9. Antioxidant activity of MB@AgNPs

Based on ascorbic acid as the reference, MB@AgNPs are assessed for antioxidant activity using a DPPH assay. It is a simple and cost-effective assay. The synthesized MB@AgNPs were assessed for their antioxidant activity by measuring the percent inhibition of DPPH radicals in the presence of ascorbic acid.[52] DPPH exhibits a high degree of hydrogen atom acceptance from antioxidant materials, so it is considered the most stable nitrogen-centred free radical. When AgNPs were added to the DPPH solution, the colour of DPPH changed, which was caused by hydrogen scavenging to form yellow-coloured DPPH. The inhibition activity of MB@AgNPs was compared to that of ascorbic acid (standard) in Fig. 10. The amount of silver nanoparticles significantly enhanced DPPH radical inhibition. Concentrations of 5, 10, 15, 20, 25 and 30 µL showed a scavenging rate of 22.5, 46.2, 55.45, 60.7, 63.6 and 62.9%, respectively. With the increased quenching rate of DPPH radicals, the obtained MB@AgNPs demonstrated that the MB@AgNPs have an enhanced antioxidation property.

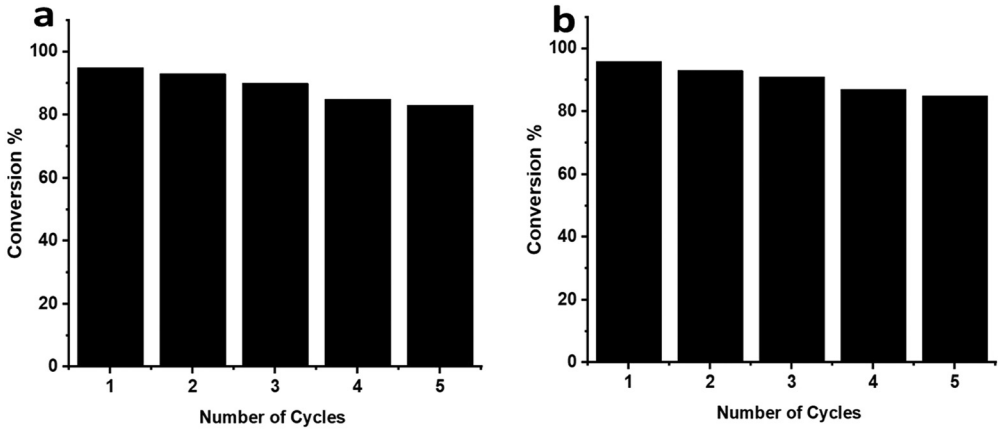

Fig. 9 The catalytic performance of MB gum stabilized AgNPs within 5 cycles towards the reduction of (a) CV and (b) Rh-B dyes.

Table 2 Antibacterial activity of MB@AgNPs at different concentrations

S. No	Micro Organism	Zone of Inhibition (mm)				
		25 μL	50 μL	75 μL	100 μL	*Streptomycin*
1	*Staphylococcus aureus*	6 mm	8 mm	10 mm	14 mm	15 mm
2	*Bacillus subtilis*	—	6 mm	7 mm	13 mm	16 mm
3	*Escherichia coli*	6	8 mm	11 mm	15 mm	16 mm
4	*Bacillus cereus*	5 mm	6 mm	8 mm	12 mm	15 mm

3.10. Antibacterial activity of MB@AgNPs

We examined the antibacterial properties of MB@AgNPs against Gram-positive (*Staphylococcus aureus* & *Bacillus subtilis*) and Gram-negative (*Escherichia coli* & *Bacillus cereus*) strains.[53] It was found that MB@AgNPs has significant antibacterial activity against pathogenic microorganisms at a concentration of 25 μL, 50 μL, 75 μL and 100 μL, respectively (Table 2). MB@AgNPs showed antibacterial activity against *Escherichia coli* & *Bacillus cereus* with a 15 and 12 mm zone of inhibition, respectively.[54] Whereas it showed antibacterial activity against *Staphylococcus aureus* and *Bacillus subtilis* with inhibition zones of 14 and 13 mm, respectively.[55] MB@AgNPs showed good antibacterial activity against *Staphylococcus aureus* and *Escherichia coli*, whereas *Bacillus subtilis* & *Bacillus cereus* showed moderate antibacterial activity. *Bacillus subtilis* and *Bacillus cereus* are spore-forming bacteria with thick peptidoglycan layers. These are highly resistant to temperature and drugs even though they are Gram-positive. These are the reasons for the moderate antibacterial activity of MB@AgNPs. Antibacterial activity was enhanced with an increase in the concentration of MB@AgNPs.

4. Conclusions

An economically viable, ultrafast, and sustainable method was established to synthesize AgNPs by M.B. gum. Increase in the concentration of $AgNO_3$, MB extract, microwave irradiation and pH enhanced the formation of MB@AgNPs. The XRD results confirmed a face-centered cubic structure. The TEM image of the MB@AgNPs showed spherical shape nanoparticles with an average size of 10 ± 2 nm. The MB@AgNPs scavenge 63% of free radicals, which makes them excellent antioxidants. CV and Rh-B dyes were catalytically reduced in 300 and 240 seconds, respectively, by MB@AgNPs in the presence of $NaBH_4$. The catalytic activity of the MB@AgNPs was dose-dependent. The MB@AgNPs showed very little loss of catalytic activity after five cycles in the reduction of CV and Rh-B dyes, which indicates the high stability of the catalyst. The results showed that MB@AgNPs have remarkable catalytic activity towards the catalytic reduction of CV and Rh-B dyes. In addition, MB@AgNPs showed good antibacterial activity with inhibition zones of 14 mm and 15 mm, respectively, against *Staphylococcus aureus* & *Escherichia coli*. The MB@AgNPs showed good to moderate antibacterial activity with inhibition zones of 13 mm and 12 mm, respectively, against *Bacillus subtilis* & *Bacillus cereus*. The results showed that MB@AgNPs have significant antibacterial activity against the tested bacterial strains. The findings of this study conclude that the synthesized MB@AgNPs are efficient, reusable, eco-friendly catalysts and well-suited for environmental remediation. Based on the obtained results of this study, MB@AgNPs can be useful in biomedicine applications such as multidrug resistance and diabetic foot wound healing.

Conflicts of interest

The authors do not have any conflicts of interest.

Acknowledgements

Dr Kondaiah Seku is greatly thankful to The Ministry of Higher Education, Research, and Innovation (MOHERI), Sultanate of Oman, for the financial support from the MOHERI Research Grant (Proposal ID: MOHERI/BFP/RGP/EBR/20/253) and Dr Ahmed I. Osman wishes to acknowledge the support from the UKRI project ''Advancing Creative Circular Economies for Plastics *via* Technological-Social Transitions'' (ACCEPT Transitions, EP/S025545/1). The KSU authors express their sincere gratitude to Researchers Supporting Project number (RSP2023 R368), King Saud University, Riyadh, Saudi Arabia. All data is provided in full in the results section of this paper.

References

1 C. Fleischmann, M. Lievenbrück and H. Ritter, *Polymers*, 2015, **7**, 717–746.
2 A. Khatri, M. H. Peerzada, M. Mohsin and M. White, *J. Clean. Prod.*, 2015, **87**, 50–57.
3 R. Kant, *Nat. Sci.*, 2012, **04**, 22–26.
4 J. C. Cardoso, G. G. Bessegato and M. V. Boldrin Zanoni, *Water Res.*, 2016, **98**, 39–46.
5 M. M. Hassan and C. M. Carr, *Chemosphere*, 2018, **209**, 201–219.
6 V. Buscio, M. Crespi and C. Gutiérrez-Bouzán, *Desalin. Water Treat.*, 2016, **57**, 8090–8096.
7 N. H. Phan, S. Rio, C. Faur, L. Le Coq, P. Le Cloirec and T. H. Nguyen, *Carbon*, 2006, **44**, 2569–2577.
8 R. Kumar, A. Umar, R. Kumar, M. S. Chauhan, G. Kumar and S. Chauhan, *Eng. Sci.*, 2021, **16**, 288–300.
9 A. J. Kora and L. Rastogi, *Arab. J. Chem.*, 2018, **11**, 1097–1106.
10 K. Seku, B. R. Gangapuram, B. Pejjai, M. Hussain, S. S. Hussaini, N. Golla and K. K. Kadimpati, *Chem. Pap.*, 2019, **73**, 1695–1704.
11 M. R. Axet and K. Philippot, *Chem. Rev.*, 2020, **120**, 1085–1145.
12 R. B. Rajput, S. N. Jamble and R. B. Kale, *Eng. Sci.*, 2022, **17**, 176–184.
13 F. Wei, H. Zhang, Q. Ren, H. Chen, L. Yang, B. Ding, M. Yu and Z. Liang, *PLoS One*, 2021, **16**, 1–12.

14 P. Balaraman, B. Balasubramanian, D. Kaliannan, M. Durai, H. Kamyab, S. Park, S. Chelliapan, C. T. Lee, V. Maluventhen and A. Maruthupandian, *Waste Biomass Valorization*, 2020, **11**, 5255–5271.
15 S. R. Prasad, S. B. Teli, J. Ghosh, N. R. Prasad, V. S. Shaikh, G. M. Nazeruddin, A. G. Al-Sehemi, I. Patel and Y. I. Shaikh, *Eng. Sci.*, 2021, **16**, 90–128.
16 K. Naseem, R. Begum, W. Wu, A. Irfan, J. Nisar, M. Azam and Z. H. Farooqi, *Int. J. Environ. Sci. Technol.*, 2021, **18**, 1809–1820.
17 I. Hussain, Z. H. Farooqi, F. Ali, R. Begum, A. Irfan, W. Wu, X. Wang, M. Shahid and J. Nisar, *J. Mol. Liq.*, 2021, **335**, 116106.
18 I. Hussain, F. Ali, M. Shahid, R. Begum, A. Irfan, W. Wu, S. Shaukat and Z. H. Farooqi, *Appl. Organomet. Chem.*, 2021, **35**, 1–13.
19 R. Begum, G. Ahmad, J. Najeeb, W. Wu, A. Irfan, M. Azam, J. Nisar and Z. H. Farooqi, *Chem. Phys. Lett.*, 2021, **763**, 138263.
20 Y. Qu, X. Pei, W. Shen, X. Zhang, J. Wang, Z. Zhang, S. Li, S. You, F. Ma and J. Zhou, *Phys. E*, 2017, **88**, 133–141.
21 K. Seku, B. R. Gangapuram, B. Pejjai, K. K. Kadimpati and N. Golla, *J. Nanostructure Chem.*, 2018, **8**, 179–188.
22 T. Feng, Z. B. Gu and Z. Y. Jin, *Food Sci. Technol. Int.*, 2007, **13**, 55–61.
23 K. Seku, S. S. Hussaini, M. Hussain, M. A. Siddiqui, N. Golla, D. Ravinder and B. Reddy G, *Phys. E*, 2022, **140**, 115169–115177.
24 A. Roy, O. Bulut, S. Some, A. K. Mandal and M. D. Yilmaz, *RSC Adv.*, 2019, **9**, 2673–2702.
25 K. Seku, S. S. Hussaini, B. Pejjai, M. M. S. Al Balushi, R. Dasari, N. Golla and G. B. Reddy, *Chem. Pap.*, 2020, 1–14.
26 K. Kasinathan, K. Marimuthu, B. Murugesan, S. Samayanan, Y. Cai and C. Rathinam, *J. Mol. Liq.*, 2021, **335**, 116582.
27 A. Activities.
28 K. Seku, S. Sulaiman Hussaini, N. Golla, G. Mangatayaru K, S. M. V. D, S. Rapolu, R. Bandi and B. Reddy G, *Mater. Lett.*, 2020, **278**, 128427–128430.
29 M. Anandan, G. Poorani, P. Boomi, K. Varunkumar, K. Anand, A. A. Chuturgoon, M. Saravanan and H. Gurumallesh Prabu, *Process Biochem.*, 2019, **80**, 80–88.
30 F. B. Araruna, T. M. de Oliveira, P. V. Quelemes, A. R. de Araújo Nobre, A. Plácido, A. G. Vasconcelos, R. C. M. de Paula, A. C. Mafud, M. P. de Almeida, C. Delerue-Matos, Y. P. Mascarenhas, P. Eaton, J. R. de Souza de Almeida Leite and D. A. da Silva, *Carbohydr. Polym.*, 2020, **241**, 115260–115269.
31 B. R. Ganapuram, M. Alle, R. Dadigala, A. Dasari, V. Maragoni and V. Guttena, *Int. Nano Lett.*, 2015, **5**, 215–222.
32 A. J. Kora and L. Rastogi, *Ind. Crops Prod.*, 2016, **81**, 1–10.
33 A. D. Mare, C. N. Ciurea, A. Man, M. Mareş, F. Toma, L. Berţa and C. Tanase, *Plants*, 2021, **10**, 2153–2167.
34 G. Singh, M. Kumar, M. Singh and R. Vaish, *J. Am. Ceram. Soc.*, 2021, **104**, 1237–1246.
35 K. Seku, G. Bhagavanth Reddy, S. S. Hussaini, B. Pejjai, M. Hussain, D. M. Reddy, M. A. K. Khazaleh and G. Mangatayaru, *Int. J. Biol. Macromol.*, 2022, **209**, 912–922.
36 S. Ameen, M. S. Akhtar, M. Nazim and H. S. Shin, *Mater. Lett.*, 2013, **96**, 228–232.
37 A. K. Gupta, A. Pal and C. Sahoo, *Dyes Pigm.*, 2006, **69**, 224–232.
38 V. Seerangaraj, S. Sathiyavimal, S. N. Shankar, J. G. T. Nandagopal, P. Balashanmugam, F. A. Al-Misned, M. Shanmugavel, P. Senthilkumar and A. Pugazhendhi, *J. Environ. Chem. Eng.*, 2021, **9**, 105088.
39 R. W. R. Santana, A. E. B. Lima, L. K. C. de Souza, E. C. S. Santos, C. C. Santos, A. S. de Menezes, S. K. Sharma, L. S. Cavalcante, M. E. H. Maia da Costa, T. O. Sales, C. Jacinto, G. E. Luz and M. A. P. Almeida, *J. Phys. Chem. Solids*, 2023, **173**, 111093.
40 R. Jain, M. Mathur, S. Sikarwar and A. Mittal, *J. Environ. Manage.*, 2007, **85**, 956–964.
41 S. Kumar, S. K. Sharma, R. D. Kaushik and L. P. Purohit, *Mater. Today Chem.*, 2021, **20**, 100464.
42 N. Alikhani, M. Hekmati, B. Karmakar and H. Veisi, *Inorg. Chem. Commun.*, 2022, **139**, 109351.
43 H. Veisi, P. Abassi, P. Mohammadi, T. Tamoradi and B. Karmakar, *Sci. Rep.*, 2021, **11**, 1–17.
44 M. Ismail, M. I. Khan, S. B. Khan, K. Akhtar, M. A. Khan and A. M. Asiri, *J. Mol. Liq.*, 2018, **268**, 87–101.
45 S. Hemmati, M. M. Heravi, B. Karmakar and H. Veisi, *J. Mol. Liq.*, 2020, **319**, 114302.
46 R. Banu, D. Ramakrishna, G. B. Reddy, G. Veerabhadram and K. G. Mangatayaru, *Mater. Today Proc.*, 2020, **43**, 2265–2273.
47 D. Baruah, M. Goswami, R. N. S. Yadav, A. Yadav and A. M. Das, *J. Photochem. Photobiol., B*, 2018, **186**, 51–58.
48 M. Ismail, M. I. Khan, M. A. Khan, K. Akhtar, A. M. Asiri and S. B. Khan, *Appl. Organomet. Chem.*, 2019, **33**, e4971.
49 P. Chawla, N. Kumar, A. Bains, S. B. Dhull, M. Kumar, R. Kaushik and S. Punia, *Int. J. Biol. Macromol.*, 2020, **146**, 232–242.
50 R. Dobrucka, *Saudi J. Biol. Sci.*, 2019, **26**, 31–37.
51 E. Murugan, S. Santhosh Kumar, K. M. Reshna and S. Govindaraju, *J. Mater. Sci.*, 2019, **54**, 5294–5310.
52 F. Gulbagca, S. Ozdemir, M. Gulcan and F. Sen, *Heliyon*, 2019, **5**, e02980.
53 D. Borah, N. Das, N. Das, A. Bhattacharjee, P. Sarmah, K. Ghosh, M. Chandel, J. Rout, P. Pandey, N. N. Ghosh and C. R. Bhattacharjee, *Appl. Organomet. Chem.*, 2020, **34**, e5597.
54 J. Sukweenadhi, K. I. Setiawan, C. Avanti, K. Kartini, E. J. Rupa and D. C. Yang, *S. Afr. J. Chem. Eng.*, 2021, **38**, 1–8.
55 K. Zomorodian, H. Veisi, S. M. Mousavi, M. S. Ataabadi, S. Yazdanpanah, J. Bagheri, A. P. Mehr, S. Hemmati and H. Veisi, *Int. J. Nanomed.*, 2018, **13**, 3965–3973.